JOURNAL OF MATERIALS SCIENCE 30 (1995) 4549–4555

Interface structure and mechanical properties of Al_2O_3–20 vol % ZrO_2–20 vol % SiC_w ceramic composite

F. YE, T. C. LEI, Q. C. MENG, Y. ZHOU
Department of Metals and Technology, Harbin Institute of Technology, Harbin 150001, People's Republic of China

J. Y. DAI
Institute of Metal Research, Acadamia Sinica, Shenyang, People's Republic of China

The microstructure, mechanical properties, fracture behaviour and toughening mechanisms of Al_2O_3–20 vol % ZrO_2 (2 mol % Y_2O_3)–20 vol % SiC_w ceramic matrix composite were investigated by X-ray diffraction, scanning and transmission electron microscopies, energy dispersive analysis of X-rays, high-resolution electron microscopy techniques and three-point bending tests. The results show that the Al_2O_3 matrix is simultaneously strengthened and toughened by both ZrO_2 particles and SiC whiskers. The interfacial amorphous layers between SiC whiskers and ZrO_2, and Al_2O_3 grains were observed by both TEM dark-field and high-resolution electron microscopy techniques.

1. Introduction

The brittle nature of Al_2O_3 ceramic, over the years, has prompted investigators to explore a variety of approaches to enhance its fracture toughness. The main approaches are incorporation of ZrO_2 particles and/or SiC whiskers [1–3]. The toughening is realized by tetragonal (t) to monoclinic (m) ZrO_2 phase transformation, whisker bridging and pull-out, and crack deflection. Many authors [4–5] have reported that the SiC_w–ZrO_2–Al_2O_3 composites have superior mechanical and thermal properties compared with the monotonic Al_2O_3 ceramic. Claussen *et al.* [6] concluded that the presence of SiC whiskers in SiC_w–ZrO_2–Al_2O_3 composite could result in a larger transformation zone, due to stress transfer by the whisker, therefore generating a higher toughness. However, to date, reports on the interfacial structure between SiC whisker and ceramic matrix in SiC_w–ZrO_2–Al_2O_3 composites are very few, and the interfacial characteristics have a strong influence on the toughening effects [7–9]. The object of this study was to assess the microstructure of Al_2O_3–20 vol % ZrO_2 (2 mol % Y_2O_3)–20 vol % SiC_w, expecially, the structure and chemical composition of the interface, using high-resolution electron microscopy and energy dispersive analysis of X-rays (EDAX) techniques and their effect on the mechanical properties of the composite.

2. Experimental procedure

The material used in this study was zirconia-toughened alumina (Al_2O_3 + 20 vol % ZrO_2 (2 mol % Y_2O_3)) reinforced with 20 vol % SiC whiskers. Ultrafine alumina powders, having an average grain size of about 0.1 μm, were proved to be α-Al_2O_3 by X-ray diffraction (XRD), and the chemical composition is shown in Table I. Ultrafine zirconia powders stabilized by 2 mol % Y_2O_3 with an average particle size of 0.65 μm contain nearly 34% tetragonal ZrO_2 and 66% monoclinic ZrO_2 and the chemical composition is shown in Table II. The β-SiC whiskers were supplied by Tokai Cabon. Japan, having a diameter of 0.5–1 μm and a length of 30–60 μm. The Al_2O_3–20 vol % ZrO_2 (2 mol % Y_2O_3)–20 vol % SiC_w composite were hot-pressed at 1650 °C for 1 h under a pressure of 25 MPa into 60 mm × 60 mm × 6 mm discs.

The density of the samples was measured by Archimedes' method in distilled water at 20 °C. The percentage of t-ZrO_2 in the total ZrO_2 was estimated by XRD on both the as-polished and the fractured surfaces.

Flexural strength and fracture toughness of the composite were measured in air at room temperature using an Instron 1186 machine. Flexural strength measurements were performed on bar specimens (3 mm × 4 mm × 36 mm) using a three-point bend fixture with a span of 30 mm. Fracture toughness measurements were performed on single-edge notched bar (SENB) specimens (2 mm × 4 mm × 25 mm) with a span of 16 mm, and a half-thickness notch was made using a diamond wafering blade, and K_{IC} values were determined using the method described elsewhere [4].

Fracture surfaces of the composites were examined using a Hitachi S-570 scanning electron microscope.

0022–2461 © *1995 Chapman & Hall*

TABLE I Chemical composition of Al_2O_3 powders (wt %)

Material	Al_2O_3	SiO_2	Fe_2O_3	CaO	MgO	TiO_2	HCl
Al_2O_3	99.66	< 0.01	< 0.01	< 0.01	< 0.01	< 0.01	< 0.2

TABLE II Chemical composition of ZrO_2 powders (wt %)

Material	ZrO_2	Al_2O_3	Y_2O_3	SiO_2	Fe_2O_3	Na_2O	CaO	MgO
ZrO_2 (2Y)	96.32	< 0.02	3.6	< 0.017	< 0.01	< 0.01	< 0.01	< 0.01

A Vickers hardness tester and an indentation load of 15 kg was used to introduce cracks into specimens for observing the crack propagation modes. The microstructure of the composite was characterized by TEM. Thin-foil specimens taken normal to the hot-pressing axis, were prepared by dimpling and subsequent ion-beam thinning and used to determine phase distribution and to identify possible interface reactions. In addition, a high-resolution phase-contrast imaging technique was employed in JEM-2000EX-II electron microscope to determine interface structure at atomic level resolution, and the distribution of chemical elements near the interface was measured by the EDAX technique.

3. Results and discussion

The mechanical properties of Al_2O_3–20 vol % ZrO_2 (2 mol % Y_2O_3)–20 vol %SiC_w composite are given in Table III. It can be seen that the fracture toughness of the composite (9.15 MPa $m^{1/2}$) is higher than that of both 20 vol % ZrO_2 (2 mol % Y_2O_3)–Al_2O_3 (6.78 MPa $m^{1/2}$) and 20 vol % SiC_w–Al_2O_3 composite (6.54 MPa $m^{1/2}$), and the flextural strength (725 MPa) is also higher than that of both 20 vol % ZrO_2 (2 mol % Y_2O_3)–Al_2O_3 (659 MPa) and 20 vol % SiC_w–Al_2O_3 composite (592 MPa), indicating that the combination of ZrO_2 with SiC whisker has a better effect for improving the mechanical properties of the material and, particularly, the combination ZrO_2 with SiC whisker can result in a larger toughening response than simple additives.

TABLE III Room-temperature mechanical properties of the composite

Material	Flexural strength (MPa)	Fracture toughness, (MP $m^{1/2}$)
$SiC_w/ZrO_2/Al_2O_3$	725 ± 45	9.15 ± 0.80

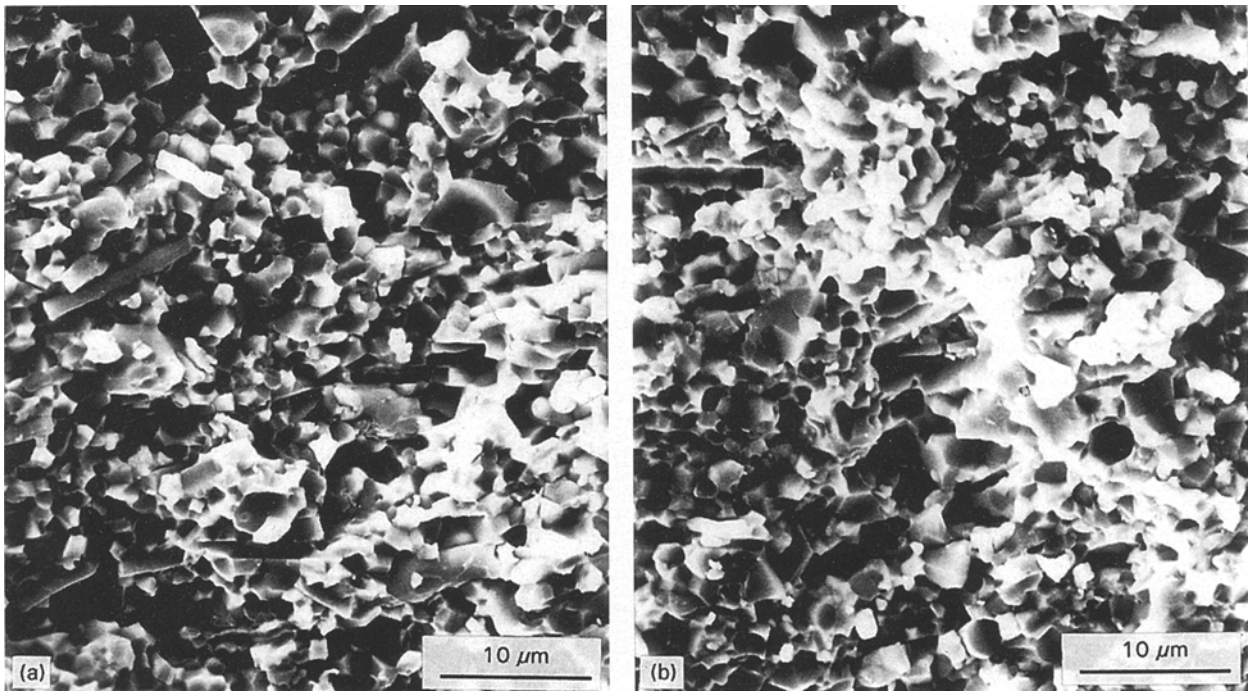

Figure 1 Fracture surfaces of SiC_w–ZrO_2 (2Y)–Al_2O_3 composite.

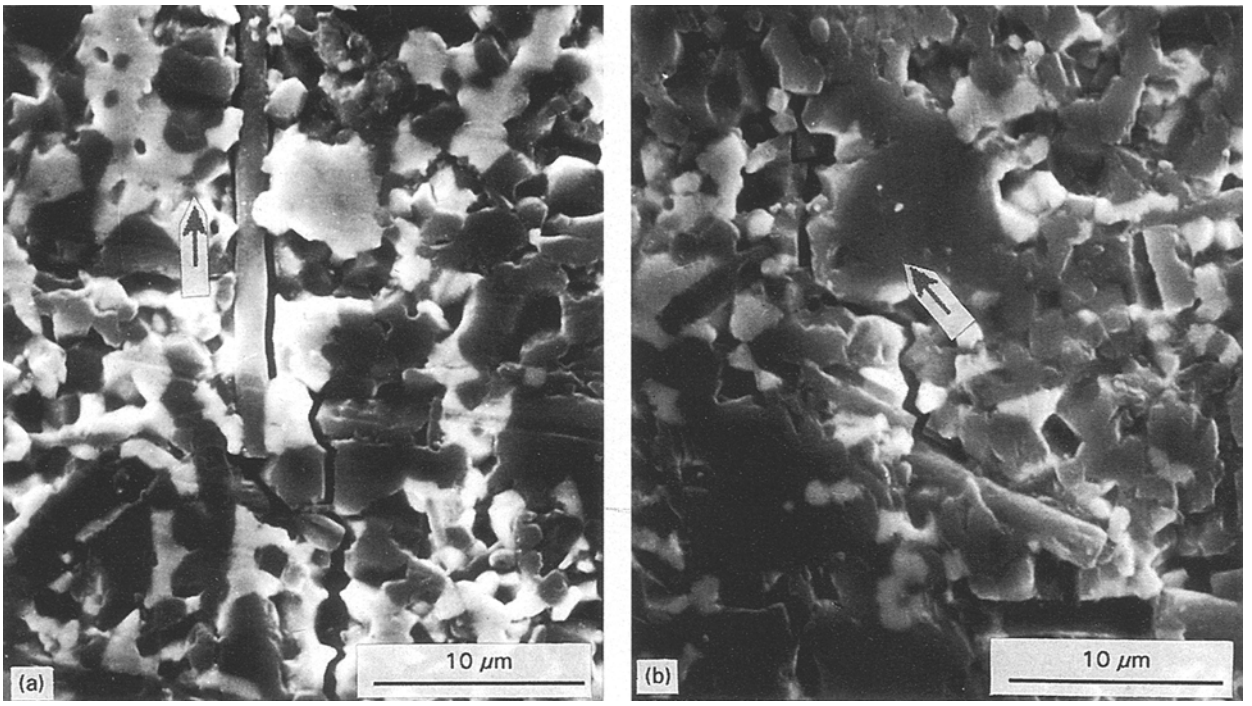

Figure 2 Scanning electron micrographs of indentation crack propagation paths in SiC_w–ZrO_2 (2Y)–Al_2O_3 composite. (a) Crack propagated along a whisker, (b) crack deflected by a whisker.

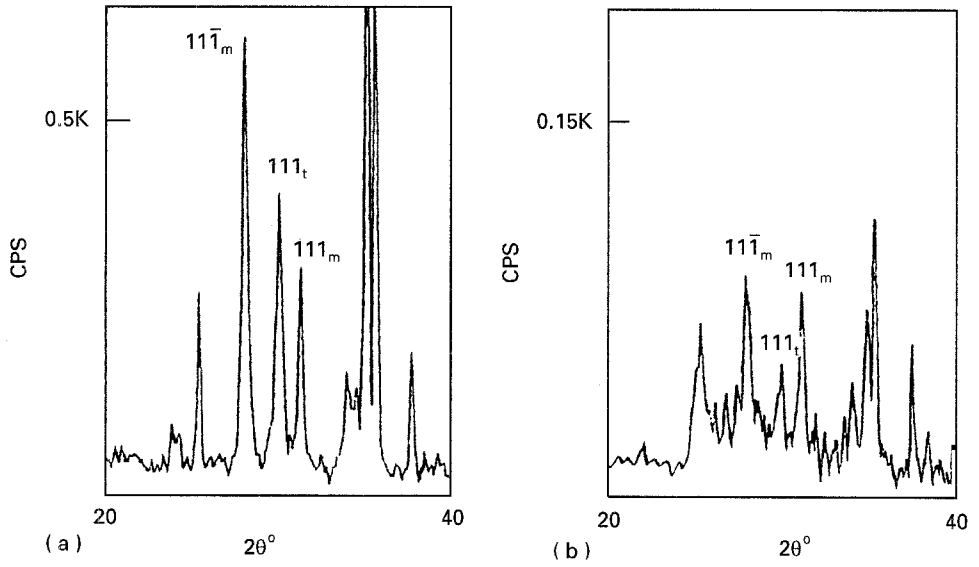

Figure 3 XRD profiles of SiC_w–ZrO_2 (2Y)–Al_2O_3 composite. (a) Polished surface (70% m–ZrO_2), (b) fractured surface (79% m–ZrO_2)

The fracture surfaces of the composite obtained after flexural strength tests are shown in Fig. 1. It appeared to be quite rough with the pulled-out whiskers and the corresponding holes left by whiskers, indicating that the crack path had been strongly deflected by the reinforcing whiskers.

The fracture mechanisms of the composite can be demonstrated more clearly by examining the crack propagation produced by a Vickers indentation. The typical crack propagation paths are shown in Fig. 2. The arrows indicate the direction of crack propagation and the effect of the whiskers on the crack path is evident. Interfacial debonding, crack bridging and whisker pull-out were commonly observed along the crack paths.

The XRD results are shown in Fig. 3, indicating the appearance of dynamic $t \rightarrow m$ ZrO_2 phase transformation during fracturing, which also contributes to the fracture toughness.

A typical structure of the composite is shown in Fig. 4. The specimen was prepared by cutting a thin section from the hot-pressed disc normal to the

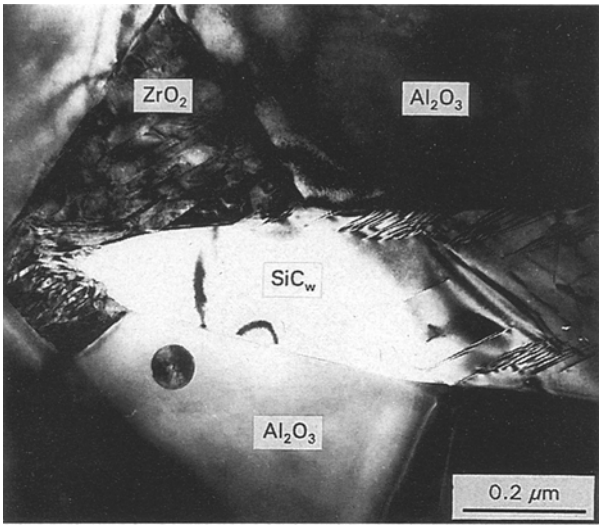

Figure 4 Transmission electron micrograph of SiC_w–ZrO_2-(2Y)–Al_2O_3 composite showing preferential alignment of the whiskers in the hot-pressing plane and good bonding between the whisker and ZrO_2 (2Y) Al_2O_3 ceramic.

pressing axis. The whiskers were seen along their axis and the serrated surfaces of the whiskers appeared to have a good bond with the ZrO_2 and Al_2O_3 grains. The ZrO_2 at the interfacial regions shows the lath structure of monoclinic phase ZrO_2 (2 mol % Y_2O_3) transformed by the induction of residual thermal stresses due to the difference in thermal expansion coefficients of the SiC whisker and ZrO_2. The stacking faults in the SiC whiskers could also be found from Fig. 4.

The microstructures of ZrO_2 and Al_2O_3 are shown in Fig. 5. The ZrO_2 particles are always located at the triple grain boundaries of Al_2O_3, except for a few ZrO_2 particles with very small grain sizes which exist within the Al_2O_3 grains. These fine ZrO_2 particles are always t-ZrO_2 because their grain sizes are much smaller than the critical size for t → m ZrO_2 transformation. The ZrO_2 particles within the Al_2O_3 grains strengthen the matrix, due to the induction of many dislocations in Al_2O_3 grains caused by elastic and thermal mismatch between ZrO_2 and Al_2O_3. The microcracks at Al_2O_3 grain boundaries can also be found in Fig. 5d, which are caused by t → m ZrO_2

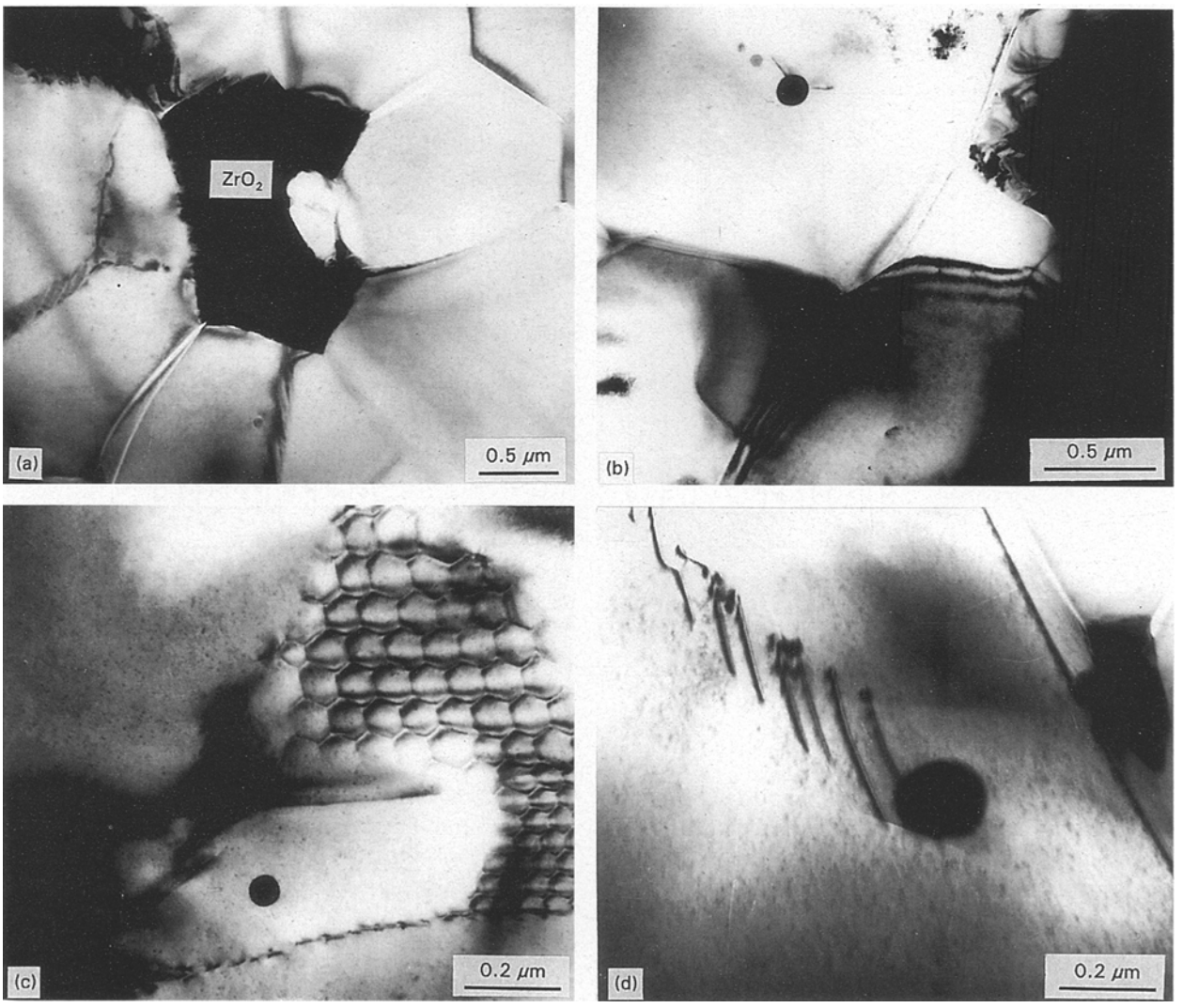

Figure 5 Transmission electron micrographs of ZrO_2 (2Y) and Al_2O_3 in SiC_w–ZrO_2 (2Y)–Al_2O_3 composite showing (a) that the ZrO_2 particles are always located at the triple grain boundaries of Al_2O_3, (b) that the ZrO_2 particles with small grain size exist in the Al_2O_3 grain, (c) the hexagonal network of dislocations in an Al_2O_3 grain, and (d) that the dislocation was pinned by ZrO_2 particles.

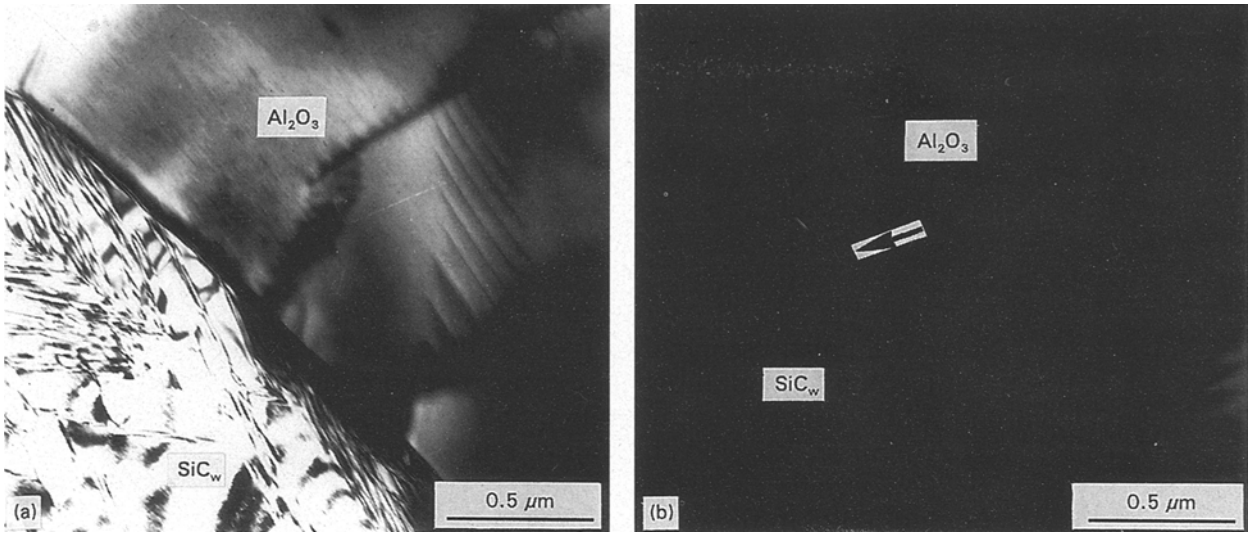

Figure 6 Transmission electron micrographs of the SiC_w–Al_2O_3 interface. (a) Bright-field image showing that the Al_2O_3 grains have a good bond with the SiC whiskers. (b) Dark-field image formed with diffusely scattered electron showing a thin layer of amorphous phase at the interface.

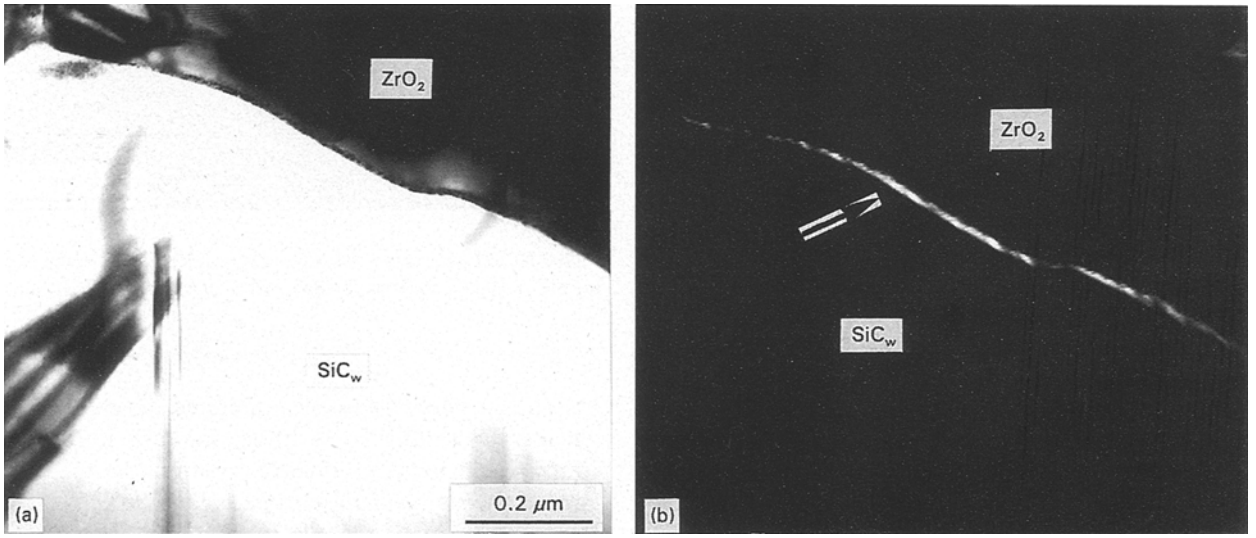

Figure 7 Transmission electron micrographs of the SiC_w–ZrO_2 interface. (a) Bright-field image showing that the ZrO_2 grains have a good bond with the SiC whiskers. (b) Dark-field image formed with diffusely scattered electron showing a thin layer of amorphous phase at the interface.

phase transformation during cooling after hot pressing. All these factors will affect the final mechanical properties of the composite.

In regions of intimate contact between the SiC whiskers and the Al_2O_3 grains (Fig. 6a), the Al_2O_3 grains have a good bond with the SiC whiskers. The dark-field image, taken with diffusely scattered electrons, highlighted a thin layer of amorphous phase at the Al_2O_3–SiC interface (arrowed in Fig. 6b). Similarly, the ZrO_2 grains and SiC whiskers are also separated by a thin layer of amorphous phase, as shown in Fig. 7. The stability of the SiC whiskers in the composite was confirmed by the X-ray diffraction spectrum (Fig. 8), which showed only the SiC, ZrO_2 and Al_2O_3 reflections.

The results of EDAX chemical analyses performed on interfaces between SiC whiskers and ZrO_2, Al_2O_3 grains are shown in Fig. 9. For two kinds of interfaces, the silicon content on the SiC side is over 95 wt % and there is little zirconium, yttrium and aluminium due to the ion thining. However, the yttrium content on the ZrO_2 side is higher than that in the original ZrO_2 (2 mol % Y_2O_3) powders and there is very small amount of silicon on the ZrO_2 side near the interface, indicating the mixture diffusion between ZrO_2 and Al_2O_3. Ricoult's [10] study on the oxidation of ZrO_2–Al_2O_3 composite indicates that oxygen atoms react with SiC, forming SiO_2 amorphous phase and graphitic carbon.

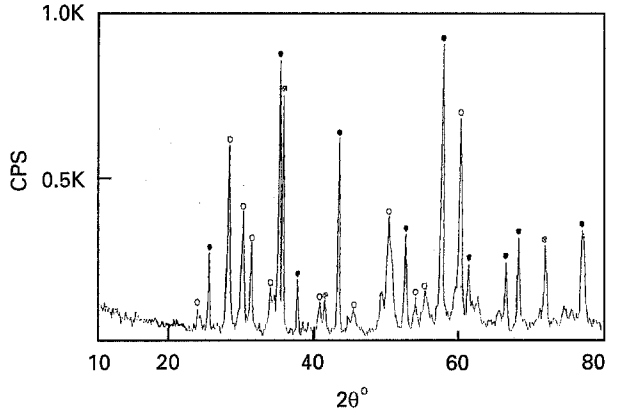

Figure 8 X-ray diffraction spectrum of SiC_w–ZrO_2 (2Y)–Al_2O_3 composite showing only (⊗) SiC_w, (○) ZrO_2 and (●) Al_2O_3 reflections.

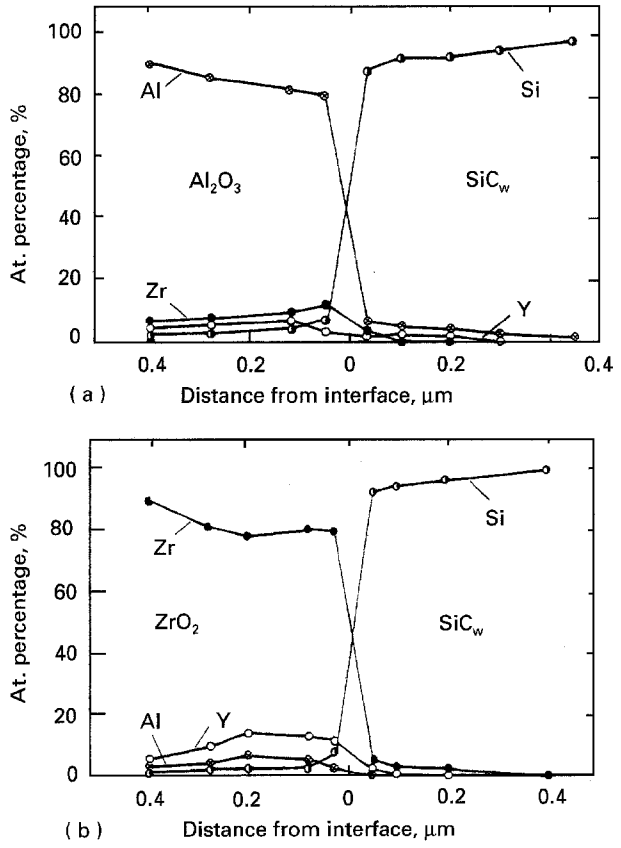

Figure 9 EDAX chemical analyses performed on the interfaces. (a) SiC_w–Al_2O_3 interface, (b) SiC_w–ZrO_2 interface.

A typical HREM image of the interface is shown in Fig. 10, indicating that Al_2O_3 and SiC are separated by a layer of amorphous phase with a thickness of nearly 10 nm (Fig. 10a). The ZrO_2/SiC_w interface also has an amorphous layer, as shown in Fig. 10b. It can also be found that the amorphous layer at the Al_2O_3–SiC_w interface is thicker than that at ZrO_2–SiC_w. The chemical composition and formation mechanism of the interfacial amorphous layer will be investigated in more detail.

The presence of the amorphous phase at the whisker/ceramic interface evidently increased the

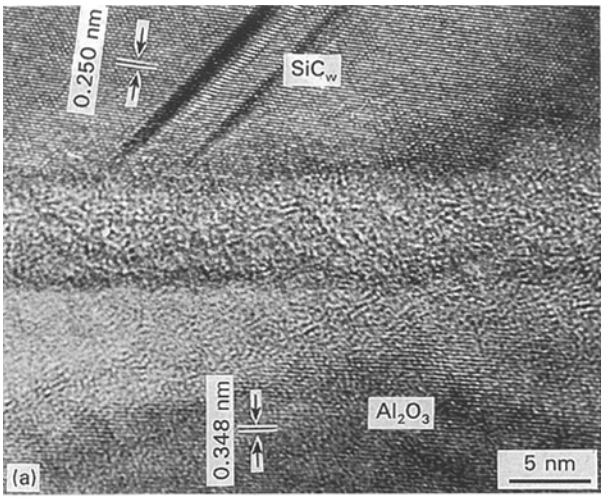

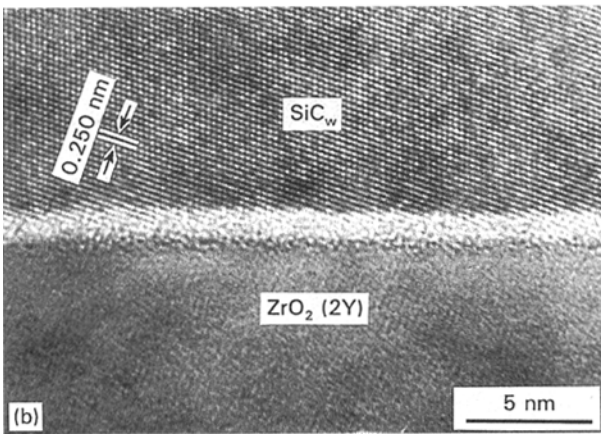

Figure 10 HREM images of SiC_w–ZrO_2 (2Y)–Al_2O_3 composite. (a) SiC_w–Al_2O_3 interface, (b) SiC_w–ZrO_2 interface.

bonding strength and hence inhibited the pull-out of whiskers, resulting in a lower fracture toughness. Many researchers [5, 11] have reported that the presence of the interfacial amorphous layer inhibited the toughening effects of SiC whiskers. The amorphous layer at the interface may be caused by the Y_2O_3 sintering aid and the light-element enrichment on the surface of the as-received whiskers. Yang and Stevens [8] have reported that the interfacial amorphous phases were virtually eliminated when the whiskers were leached with an acid before being incorporated into the matrix. As shown in Figs 1 and 2, both the numbers and length of pulled-out whiskers are limited, which are directly affected by the interfacial amorphous layer. Therefore, the pre-treatment of whiskers may be one of the effective approaches to eliminate the interfacial amorphous phases between SiC whiskers and the ceramic matrix for improving the fracture toughness of the composites.

4. Conclusions

1. The combination of ZrO_2 with SiC whisker has a good effect for improving the mechanical properties of Al_2O_3 matrix. The main toughening mechanisms of the composite are crack deflection, whisker bridging,

whisker pull-out and t → m ZrO_2 phase transformation.

2. SiC whiskers and ZrO_2, Al_2O_3 grains are separated by an interfacial layer of amorphous phase, which inhibit the pull-out of whiskers.

3. Elemental mixture diffusion occurs between ZrO_2 and Al_2O_3 grains in SiC_w–ZrO_2–Al_2O_3 composites.

References

1. Q. L. GE, PhD dissertation Harbin Institute of Technology, People's Republic of China (1992) in Chinese.
2. G. Y. LIN, PhD dissertation Harbin Institute of Technology, People's Republic of China (1993) in Chinese.
3. A. G. EVANS *Mater. Sci. Res.* **21** (1987) 775.
4. P. F. BECHER and T. N. TIEGS, *J. Am. Ceram. Soc.* **70** (1987) 651.
5. N. CLAUSSEN and G. PETZOW *Mater. Sci. Res.* **20** (1986) 649.
6. N. CLAUSSEN, K. L. WISSKOPF and M. RUHLE, *J. Am. Ceram. Soc.* **69** (1986) 288.
7. J. J. BRENNAN and S. R. NUTT, *ibid.* **75** (1992) 1250.
8. M. YANG and R. STEVEN, *J. Mater. Sci.* **26** (1991) 726.
9. P. F. BECHER, C. H. HSUEH, F. ANGELINI and T. N. TIEGS, *J. Am. Ceram. Soc.* **71** (1988) 1050.
10. M. B. RICOULT *ibid.* **74** (1991) 1793.
11. N. CLAUSSEN and G. RETZOW, *Mater. Sci. Res.* **20** (1986) 549.

Received 4 August 1994
and accepted 21 February 1995